The 8th European Congress on Computational Methods in Applied Sciences and Engineering
ECCOMAS Congress 2022
5-–9 June 2022, Oslo, Norway

MULTI-FIDELITY ACTIVE LEARNING FOR SHAPE OPTIMIZATION PROBLEMS AFFECTED BY NOISE

JEROEN WACKERS[1], RICCARDO PELLEGRINI[2], ANDREA SERANI[2], MATTEO DIEZ[2], AND MICHEL VISONNEAU[1]

[1] LHEEA Lab, Ecole Centrale de Nantes, CNRS UMR 6598
1 rue de la Noë, B.P. 92101, 44321 Nantes cedex 3, France
e-mail: jeroen.wackers@ec-nantes.fr

[2] CNR-INM, National Research Council – Institute of Marine Engineering
Via di Vallerano 139, 00128 Rome, Italy

Key words: Active learning, Multi-fidelity, Shape optimization, Mesh adaptation, Simulation noise

Abstract. The efficiency of simulation-driven design optimization based on surrogate models, depends strongly on the suitability of the surrogate model for the simulation data on which it is based. We investigate adaptive surrogate modelling methods that maximize the efficiency and the robustness for any optimization problem. Specific techniques include: adaptive sampling, noise filtering by metamodel tuning, and small initial datasets to give maximum freedom to the adaptation. These methodological advancements are demonstrated for an analytical test problem, as well as the shape optimization of the DTMB 5415 ship model for calm-water resistance.

1 INTRODUCTION

In naval engineering, simulation-driven design optimization (SDDO) is continuously growing in popularity, because it allows the designers to explore innovative designs and to better assess the designs' performance in the intended operational environment. The effectiveness of SDDO comes from the tight integration of (a) mathematical models, from analytical models to numerical simulations, to evaluate the design performance, (b) highly controllable shape deformation techniques, and (c) effective optimization algorithms (global/local and derivative-based/derivative free algorithms). And yet, accurate performance predictions for innovative configurations or off-design conditions require high-fidelity physics-based models, such as CFD simulations. Furthermore, the number of iterations required by an optimization algorithm to converge, may imply performing a significant number of simulations, especially if a global optimum is desired. As a consequence, the computational requirements (such as hardware and/or computational time) may easily become unaffordable for most users. The cost associated with SDDO may be reduced by supervised machine learning via surrogate modeling methods. Here, a surrogate model is trained on the responses from a limited number of simulations and the optimization is then performed over the surrogate model, which is cheap to evaluate. Among these methods, multi-fidelity (MF) approaches are gaining attention, due to their capability to combine the accuracy of high-fidelity solvers with the computational cost of low-fidelity solvers.

Different fidelities for the input data may be defined based for example on the physical model [1] or spatial and/or temporal discretization [11]. These data are combined into one surrogate model, by correcting a low-fidelity model using suitable error metamodels (or bridge functions) which represent the difference between fidelity levels, ordered following a given hierarchy. The resulting MF surrogate is then explored by the optimization algorithm.

The efficiency and the robustness of a multi-fidelity active learning approach depend strongly on its suitability for the specific problem being modeled. Since surrogate models have many free parameters and modelling choices, a practically useable method requires automated, adaptive tuning and selection of these parameters for each specific design optimization, see *e.g.* [12, 7]. The present authors' work on MF active learning and model auto-tuning includes adaptive sampling of the datapoints [10], noise reduction through tuned least-squares fitting of the surrogate models [15], the use of more than two fidelity levels [14], and reduced initial datasets to provide maximum freedom to the adaptation [5].

The objective of the paper is to present the authors' current adaptive multi-fidelity active learning approach. The performance of the method is evaluated using an analytical test and a SDD case based on computational fluid dynamics (CFD) simulations, namely the shape optimization of the DTMB 5415 ship model, for which different fidelity levels are provided by CFD with adaptive grid refinement. Under the assumption of a limited budget of function evaluations, the proposed MF method shows better performance in comparison with less sophisticated MF models.

2 MULTI-FIDELITY ACTIVE LEARNING METHOD

2.1 Multi-fidelity setting

Consider $\mathbf{x} \in \mathbb{R}^D$ as a design variables vector of dimension D. Let the true merit function to be optimized $f(\mathbf{x})$, be assessed by N fidelity levels: the highest-fidelity level is $f_1(\mathbf{x})$, the lowest-fidelity is $f_N(\mathbf{x})$, and the intermediate fidelity levels are $\{f_i\}_{i=2}^{N-1}(\mathbf{x})$. Using $\widetilde{\cdot}$ to denote surrogate model prediction and $\widehat{\cdot}$ for multi-fidelity prediction, the MF approximation $\widehat{f}_i(\mathbf{x})$ of $f_i(\mathbf{x})$ $(i = 1, \ldots, N-1)$ is the sum of the lowest-fidelity surrogate and surrogates of the errors (inter-level errors or bridge-functions, $\widetilde{\varepsilon}$) between subsequent levels

$$\widehat{f}_i(\mathbf{x}) = \widetilde{f}_N(\mathbf{x}) + \sum_{k=i}^{N-1} \widetilde{\varepsilon}_k(\mathbf{x}). \tag{1}$$

For each i-th fidelity level the training set is $\mathcal{T}_i = \{\mathbf{x}_j, f_i(\mathbf{x}_j)\}_{j=1}^{J_i}$, with J_i the training set size. The resulting inter-level error training set is defined as $\mathcal{E}_i = \{\mathbf{x}_j, \varepsilon_i(\mathbf{x}_j)\}_{j=1}^{J_i}$, where

$$\varepsilon_i(\mathbf{x}_j) = f_i(\mathbf{x}_j) - \widehat{f}_{i+1}(\mathbf{x}_j). \tag{2}$$

The surrogate models are based on stochastic radial basis functions (SRBF) which provide both the prediction and its associated uncertainty [12]. If the uncertainty $U_{\widetilde{f}_N}$ of the lowest-fidelity prediction is uncorrelated with the uncertainty $U_{\widetilde{\varepsilon}_k}$ of the inter-level error predictions,

the uncertainty $U_{\widehat{f}_i}$ of the MF prediction can be evaluated as $(i = 1, \ldots, N-1)$

$$U_{\widehat{f}_i}(\mathbf{x}) = \sqrt{U^2_{\widetilde{f}_N}(\mathbf{x}) + \sum_{k=i}^{N-1} U^2_{\widetilde{\varepsilon}_k}(\mathbf{x})}. \tag{3}$$

2.2 Stochastic radial basis functions with least squares approximation

Given a (single-fidelity) training set $\mathcal{T} = \{\mathbf{x}_i, f(\mathbf{x}_i)\}_{i=1}^{J}$, the SRBF surrogate model prediction $\widetilde{f}(\mathbf{x})$ is computed as the expected value (EV) over a stochastic tuning parameter of the surrogate model [12], $\tau \sim \text{unif}[1, 3]$

$$\begin{aligned} \widetilde{f}(\mathbf{x}) &= \text{EV}\left[g(\mathbf{x}, \tau)\right]_\tau, \\ g(\mathbf{x}, \tau) &= \text{EV}\left[\mathbf{f}\right] + \sum_{j=1}^{M} w_j ||\mathbf{x} - \mathbf{c}_j||^\tau, \end{aligned} \tag{4}$$

where w_j are unknown coefficients, $||\cdot||$ is the Euclidean norm and $\mathbf{c}_j$ are the RBF centers, with $j = 1, \ldots, M$ and $M \leq J$. Noise reduction in the training set is achieved by choosing a number of RBF centers M smaller than the number of training points J, and $\mathbf{c}_j$ coordinates are defined via k-means clustering [4] of the training points coordinates. w_j are determined with least squares regression by solving $\mathbf{w} = (\mathbf{A}^\mathsf{T}\mathbf{A})^{-1}\mathbf{A}^\mathsf{T}(\mathbf{f} - \text{EV}\left[\mathbf{f}\right])$. The optimal number of stochastic RBF centers ($M^\star$) is defined by minimizing a leave-one-out cross-validation (LOOCV) metric [15].

2.3 Initial training set and bounded surrogate model

The reduced training set (RS) of [5] is used: except on the lowest fidelity level, where the domain center and the centers of the boundary faces are sampled, the metamodels are initialized with only a point in the domain center. For the error metamodels, this requires a SRBF surrogate which can handle extrapolation. Therefore, a bounded surrogate model prediction and uncertainty (both identified with the B subscript) for the error metamodels are defined as described in Algorithm 1. The definition of $U_{\widetilde{\varepsilon}_{Bi}}(\mathbf{x})$ stems from the consideration that the error surrogates represent errors in the MF approximation $\widehat{f}$. Therefore the average error can be used as reference for the surrogate model prediction uncertainty when an extrapolation is performed.

In Algorithm 1 a sigmoid-like function $s(r)$ is used to provide a smooth transition between the SRBF prediction and the bounded prediction

$$s(r) = \frac{1}{1 + e^{\alpha(r-\gamma)}}, \tag{5}$$

where, for the present work, $\alpha = -75$ and $\gamma = 0.2$. To define r, the smallest hyperrectangle (whose edges are parallel to the Cartesian coordinated axis) containing the training points is defined and r is the Euclidean distance of $\mathbf{x}$ from the hyperrectangle boundaries.

2.4 Active learning method

The MF surrogate model is dynamically updated by adding new training points. First, a new training point $\mathbf{x}^\star$ is identified based on the aggregate-criteria active learning (ACAS, see Fig.

Algorithm 1: Bounding of the SRBF prediction and the associated uncertainty for the error metamodels.

if $J_i = 1$, $i = 1, \ldots, N-1$ **then** // One training point available
  $\widetilde{\varepsilon}_{Bi}(\mathbf{x}) = \varepsilon(\mathbf{x}_1)$;
  $U_{\widetilde{\varepsilon}_{Bi}}(\mathbf{x}) = \varepsilon(\mathbf{x}_1)$;
else if $J_i > 1$, $i = 1, \ldots, N-1$ **then** // J_i training points available
  $\widetilde{\varepsilon}_{Bi}(\mathbf{x}) = \widetilde{\varepsilon}_i(\mathbf{x})\,[1 - s_i(r)] + \mathrm{EV}[\varepsilon_i] s_i(r)$;
  $U_{\widetilde{\varepsilon}_{Bi}}(\mathbf{x}) = \min(U_{\widetilde{\varepsilon}_i}, \mathrm{EV}\varepsilon_i])$;
end

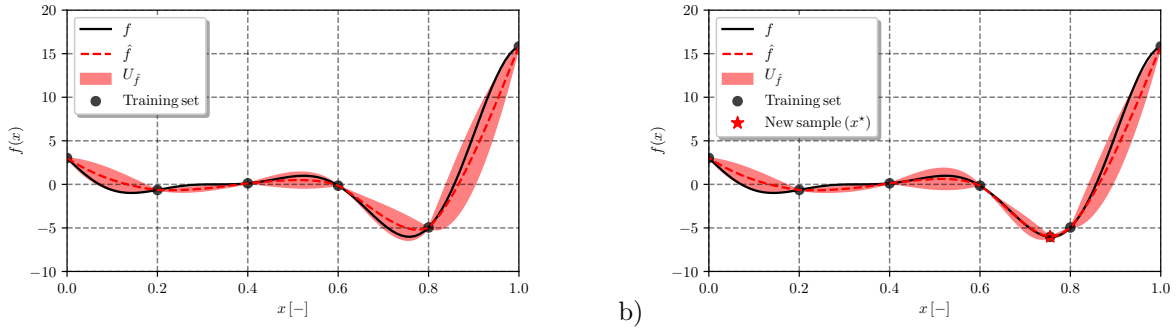

Figure 1: Example of the active learning method using one fidelity: (a) shows the initial surrogate model with the associated prediction uncertainty and training set; (b) shows the position of the new training point and the new surrogate model prediction and its uncertainty.

1) presented in [10], which samples points with large prediction uncertainty and small objective function value:

$$\mathbf{x}^\star = \underset{\mathbf{x}}{\mathrm{argmin}} \left[\widehat{f}(\mathbf{x}) - U_{\widehat{f}}(\mathbf{x}) \right], \tag{6}$$

Once $\mathbf{x}^\star$ is identified, the fidelity to be evaluated is selected. The new training point is added to the k-th training set $\mathcal{T}_k$ and to the lower-fidelity sets from $k+1$ up to N, where $k = \mathrm{maxloc}(\boldsymbol{\phi})$ and the elements of $\boldsymbol{\phi}$ for $i = 1, \ldots, N-1$ are defined as

$$\phi_i = \begin{cases} \dfrac{\sqrt{U^2_{\widehat{\varepsilon}_i} - \mathrm{MSE}_i}}{\beta_i}, & \text{if } \mathrm{MSE}_i < U^2_{\widehat{\varepsilon}_i}, \\ \dfrac{U_{\widehat{\varepsilon}_i}}{\beta_i}, & \text{if } \mathrm{MSE}_i \geq U^2_{\widehat{\varepsilon}_i}, \end{cases} \tag{7}$$

and for $i = N$ as

$$\phi_N = \begin{cases} \dfrac{\sqrt{U^2_{\widetilde{f}_N} - \mathrm{MSE}_N}}{\beta_N} & \text{if } \mathrm{MSE}_N < U^2_{\widetilde{f}_N}, \\ \dfrac{U_{\widetilde{f}_N}}{\beta_N} & \text{if } \mathrm{MSE}_N \geq U^2_{\widetilde{f}_N}. \end{cases} \tag{8}$$

Here $\beta_i = c_i / c_1$ with c_i the computational cost associated to the i-th level and c_1 the computa-

tional cost of the highest-fidelity. MSE_i is the mean-squared error computed as

$$\mathrm{MSE}_i = \begin{cases} \frac{1}{J_i} \sum_{j=1}^{J_i} \left[\varepsilon_i(\mathbf{y}_j) - \widetilde{\varepsilon}_i(\mathbf{y}_j)\right]^2 & \text{if } i < N, \\ \frac{1}{J_N} \sum_{j=1}^{J_N} \left[f_N(\mathbf{y}_j) - \widetilde{f}_N(\mathbf{y}_j)\right]^2 & \text{if } i = N. \end{cases} \tag{9}$$

This approach aims to better distribute the available budget of function evaluations among the fidelity levels. Indeed, when the least-squares regression is accurate for a fidelity and the surrogate prediction uncertainty decreases towards the average noise variance in the training set, it is not interesting to continue sampling that fidelity level, since the surrogate prediction is already accurate compared with the noise affecting the training set. Thus, adding more (noisy) training points will not improve the metamodel accuracy.

3 HYDRODYNAMIC FLOW SOLVER

Simulations to create the input data are performed with the Navier-Stokes solver ISIS-CFD developed at ECN – CNRS, available in the FINE™/Marine computing suite from Cadence Design Systems. ISIS-CFD is an incompressible unstructured finite-volume solver for multifluid flow. The velocity field is obtained from the momentum conservation equations and the pressure field is extracted from the mass conservation constraint transformed into a pressure equation. Free-surface flow is simulated with a conservation equation for the volume fraction of water, discretized with specific compressive discretization schemes. A detailed description of the solver is given by [6].

The computational grids are created through adaptive grid refinement [13]. For the MF optimization, grid adaptation is used to take into account the need for several fidelities. The interest of this procedure is that different fidelity results can be obtained by running the same simulations and simply changing the refinement threshold, a parameter which determines the global mesh fineness. Thus, it is straightforward to automate the MF simulations. The grids for the simulation of different geometries are obtained through grid deformation [2].

4 OPTIMIZATION PROBLEMS

For the numerical tests, the MF SRBF method presented here (labeled RS-MSE) is compared with a method (labeled RS) where the correction with the MSE is removed from Eqs. (7) and (8) and with one (FS) where furthermore, the RS is replaced by a full startset on all levels. The assessment of these methods is based on an analytical test and a CFD-based design optimization problem, with design space dimension $D = 2$. The optimization is performed with a fixed budget of function evaluations: considering a normalized computational cost of a highest-fidelity evaluation (equal to 1), the overall computational cost CC is proportional to the training set sizes $\mathcal{J}_l$: $CC = \mathcal{J}_1 + \sum_{l=2}^{N} \beta_l \mathcal{J}_l$.

4.1 Analytical test problem

This is an analytical test problem affected by artificial numerical noise with $D = 2$, defined as

$$\begin{array}{ll} \text{minimize} & f(\mathbf{x}) \\ \text{subject to} & \mathbf{l} \leq \mathbf{x} \leq \mathbf{u}, \end{array} \tag{10}$$

where $l_i = 0.3$ and $u_i = 1$ (for $i = 1, \ldots, D$) are the lower and upper bound for $\mathbf{x}$, respectively, and $f(\mathbf{x})$ is approximated by $N = 2$ fidelity levels ($f_1(\mathbf{x})$ and $s_2(\mathbf{x})$) as

$$\begin{aligned} f_1(\mathbf{x}) =& \sin\left(\frac{1}{x_1 x_2}\right), \\ f_2(\mathbf{x}) =& f_1(\mathbf{x}) - 9A_2 \cos\left(\frac{1}{x_1 x_2}\right), \\ s_2(\mathbf{x}) =& f_2(\mathbf{x}) + \mathcal{N}(\mathbf{x}), \end{aligned} \tag{11}$$

with $A_2 = 0.5$, $\mathcal{N} \sim \text{unif}[-0.1R_1; 0.1R_1]$ the noise associated to the 2-nd fidelity, and $R_1 = 2$ the function range of the highest fidelity level. $f_1(\mathbf{x})$ has two loci with the same lowest value for $x_1 x_2 = 2/(3\pi)$ and $x_1 x_2 = 2/(7\pi)$, see Fig. 2a.

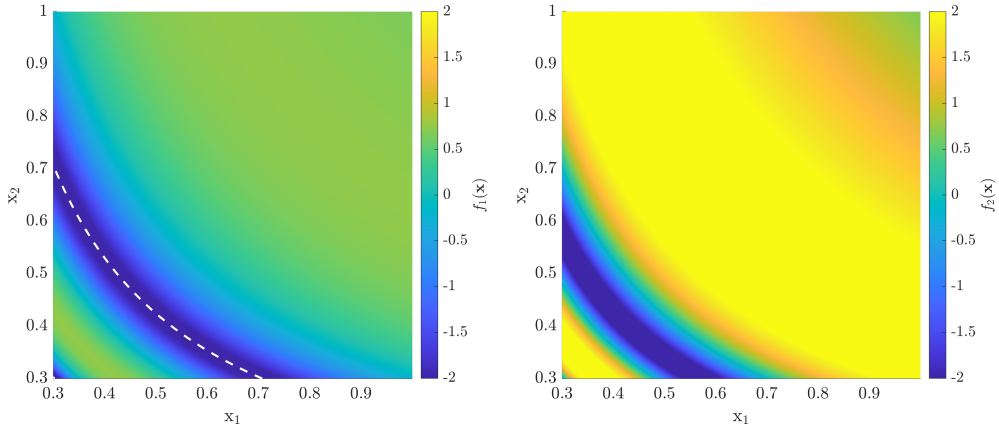

(a) High-fidelity $f_1(\mathbf{x})$ (b) Low-fidelity $f_2(\mathbf{x})$

Figure 2: Analytical test problem without artificial numerical noise. The dashed lines show the two loci with the lowest $f_1(\mathbf{x})$ value (the $x_1 x_2 = 2/(7\pi)$ locus is in the neighborhood of the bottom-right corner).

The computational cost of the analytical test problem is negligible, therefore an artificial computational cost is defined as $\beta_1 = 1$ and $\beta_2 = 0.2$. A computational budget equal to $100D$ is used. Since the noise is synthetically added to the analytical functions by a numerical generator of random numbers, a statistical analysis [3] is performed varying the seed of the random number generator for 25 repetitions.

4.2 DTMB 5415 model

The shape of the DTMB 5415 destroyer is optimized for minimal resistance R_T. The optimization problem reads

$$\begin{aligned} \text{minimize} \quad & f(\mathbf{x}) = R_T(\mathbf{x}) \\ \text{subject to} \quad & L_{pp}(\mathbf{x}) = L_{pp,0} \\ \text{and to} \quad & \mathbf{l} \leq \mathbf{x} \leq \mathbf{u}, \end{aligned} \tag{12}$$

where $L_{pp,0} = 5.72$ m (model scale) is the original length between perpendiculars. The ship is at even keel, with Froude number Fr $= 0.30$ and Re $= 1.18 \cdot 10^7$. The L_{pp} constraint is automatically satisfied by the shape modification method.

The modified geometries ($\mathbf{g}$) are produced by the linear superposition of D orthonormal basis functions ($\boldsymbol{\psi}$) on the original geometry ($\mathbf{g}_0$), as follows

$$\mathbf{g}(\boldsymbol{\xi}, \mathbf{x}) = \mathbf{g}_0(\boldsymbol{\xi}) + \boldsymbol{\delta}(\boldsymbol{\xi}, \mathbf{x}), \tag{13}$$

with

$$\boldsymbol{\delta}(\boldsymbol{\xi}, \mathbf{x}) = \sum_{k=1}^{D} x_k \boldsymbol{\psi}_k(\boldsymbol{\xi}), \tag{14}$$

where $\boldsymbol{\xi}$ are the geometry Cartesian coordinates, whereas $-1.25 \leq \{x_k\}_{k=1}^{D} \leq 1.25$ and $\{\boldsymbol{\psi_k}\}_{k=1}^{D}$ are the reduced design variables and the eigenfunctions, respectively, provided by the design-space augmented dimensionality reduction (ADR) procedure described in [8]. In the current work, two design variables are used. The simulation setup for the DTMB 5415 is provided in [14]; the cost functions are taken as $\beta_2 = 0.21$ and $\beta_3 = 0.06$.

5 NUMERICAL RESULTS

The results for the analytical problem are assessed by two error metrics [9]. Knowing the position of the global optimum $\check{\mathbf{x}}$, these metrics characterize the normalized error in the design space and the objective function space, respectively:

$$E_x \equiv \|\mathbf{x}^\star - \check{\mathbf{x}}\|, \qquad E_f \equiv \frac{f(\mathbf{x}^\star) - f(\check{\mathbf{x}})}{R_1}, \tag{15}$$

where $\mathbf{x}^\star$ is the location of the approximated optimum (normalized in unit hypercube), and R_1 is the range of the highest-fidelity level computed considering the initial FS training set. The equation for E_f uses an evaluation of the objective with the highest fidelity level at the point $\mathbf{x}^\star$ identified by the surrogate as the global optimum.

For the DTMB 5415 model problem the reference optimum is not available, therefore a different set of design-sensitive metrics are employed. These metrics quantify design point location and objective function, respectively:

$$\Delta_x \equiv \frac{\|\mathbf{x}^\star - \mathbf{x}_0\|}{\sqrt{D}}, \qquad \Delta_f \equiv \frac{f(\mathbf{x}^\star) - f(\mathbf{x}_0)}{f(\mathbf{x}_0)}, \tag{16}$$

where $\mathbf{x}_0$ is the original objective function value, meaning that Δ_x evaluates the distance of the global optimum position from the original design in the design variable space, whereas Δ_f provides the objective function variation with respect to the parent design. Additionally, a prediction error is used to quantify the error of the surrogate model in predicting the minimum value:

$$E_p = \frac{\widehat{f}(\mathbf{x}^\star) - f(\mathbf{x}^\star)}{R_1}. \tag{17}$$

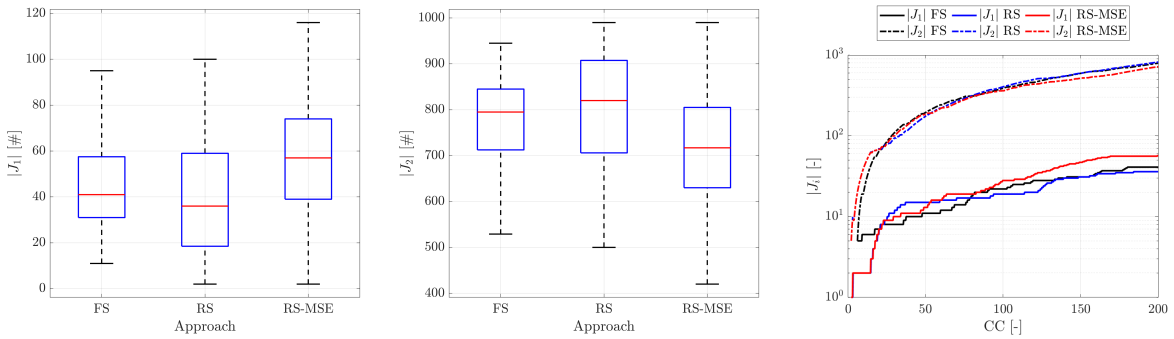

(a) $|J_1|$ (high fidelity)

(b) $|J_2|$ (low fidelity)

(c) Median of the training sets size versus CC

Figure 3: Analytical test, box plot of the training sets size and training sets sizes versus computational cost.

5.1 Analytical test problem

The challenge of this optimization test is twofold (Fig. 2): first, it has multiple optima located on the loci $x_1x_2 = 2/(3\pi)$ and $x_1x_2 = 2/(7\pi)$, and second, the LF and HF optima are in different locations, which is a danger for multi-fidelity methods which rely too heavily on LF data.

Considering the sampling approach of our three methods, in Fig. 3a-b the training set sizes are discussed using box plots. The box plot shows the q_1, q_2 (median), and q_3 quartiles, while the lower and upper whiskers are given by $q_1 - 1.5\text{IQR}$ and $q_3 + 1.5\text{IQR}$, respectively, with $\text{IQR} = q_3 - q_1$ the interquantile range. Since nested training sets are used, the number of low-fidelity samples is equal to the number of active learning iterations minus five (for the initialization). Thus, the RS approach without the forced HF sampling in the startset leads to a higher number of iterations with respect to FS, allowing a potential better exploration of the design space. Differently, the RS-MSE approach performs a lower number of iterations but uses a higher number of high-fidelity samples in comparison with FS and RS, since LF sampling is discouraged once the LF uncertainty approaches the noise level. The evolution of the sample sizes (Fig. 5c) shows the higher number of LF samples at the start (below $CC = 10$) for both RS and RS-MSE, indicating that the early exploration is performed with low-fidelity samples only. This is followed by a larger increase of HF samples for RS-MSE. Still, RS and RS-MSE have larger whiskers than FS, showing a significant variability and less consistency in the results.

Figure 4 shows the box plots of the three error metrics. The RS and RS-MSE approaches achieve lower median values than the FS approach, while RS-MSE performs the best; its median result is an almost exact optimum. Finally, the FS approach achieves the smallest IQR. Thus, FS is consistent, but it is consistently wrong: the information in the large initial sample set forces the optimization into a fixed, but suboptimal direction. RS with its greater freedom performs better, but its reliance on LF data also leads to some bad results, since the LF optimum does not correspond to the HF one; hence the large IQR for this approach. Finally, RS-MSE with its initial LF sampling and final emphasis on HF samples provides more consistently good results.

In Fig. 5 the placement of HF samples with respect to x_1x_2 is studied: the quantity c_i is

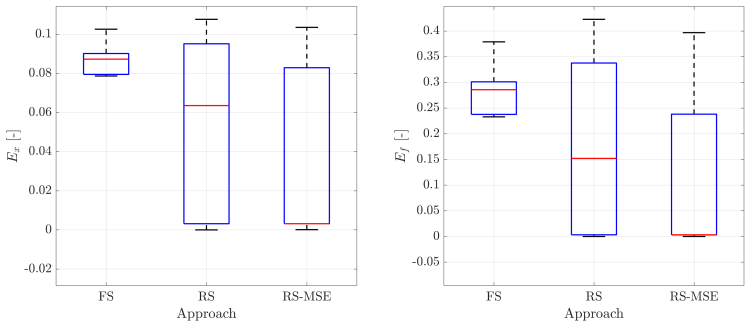

(a) E_x (b) E_f

Figure 4: Analytical test, box plots of the E_x and E_f metrics.

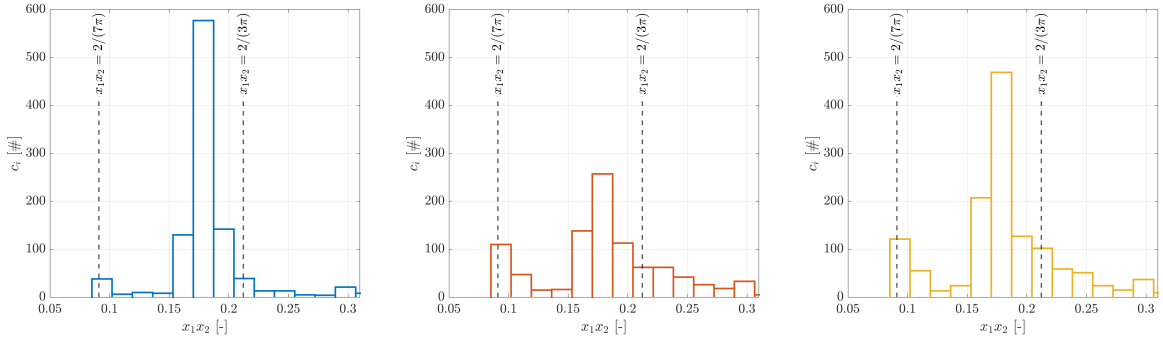

(a) x_1x_2 quantity for J_1 of FS (b) x_1x_2 quantity for J_1 of RS (c) x_1x_2 quantity for J_1 of RS-MSE

Figure 5: Analytical test, histogram of the x_1x_2 quantity for the high-fidelity training set (with c_i the number of elements in each bin).

the number of elements in each bin of width 0.017. The figure shows that FS requests most of its high-fidelity training point close to the $x_1x_2 = 2/(3\pi)$ locus and only a small quantity in the neighborhood of the $x_1x_2 = 2/(7\pi)$ locus, negatively affecting the final performance. The RS approach request almost the same quantity of high-fidelity training points between the two loci, in the position of the LF optimum. The RS-MSE approach requests for the highest number of high-fidelity training points in the $x_1x_2 = 2/(3\pi)$ locus and almost the same number of high-fidelity samples in the second locus as the RS approach. This explains why the RS-MSE approach achieves the best performance overall.

5.2 DTMB 5415 SDDO problem

Since this optimization of 3D free-surface flows is characterized by high computational costs, the problem is solved only with the RS-MSE approach. The comparison with the FS approach is provided taking the results presented in [15]. Since both the adaptive metamodelling strategy and the CFD simulations have changed, this does not provide a detailed assessment of one topic;

rather, the comparison globally shows the progress that has been achieved in the last two years.

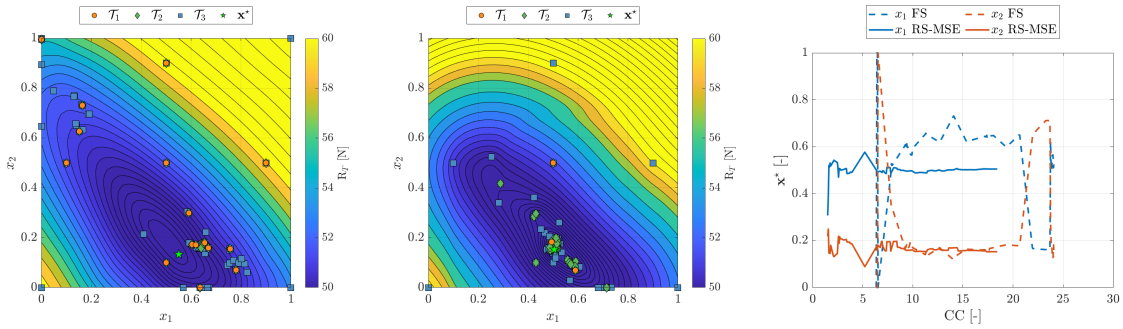

(a) FS, R_T prediction (b) RS-MSE, R_T prediction (c) $\mathbf{x}^\star$ convergence

Figure 6: DTMB 5415 SDDO problem, multi-fidelity surrogate model prediction and $\mathbf{x}^\star$ convergence for the FS and RS-MSE approaches.

Figure 6a-b present the multi-fidelity surrogate models at the last iteration of the active learning approach, the MF datasets, and the predicted optima. The sampling strategies for the two approaches are radically different: RS-MSE performed an exploration of the domain using only low-fidelity samples, correctly identifying the minimum region. The precision in this region is then increased using mainly medium-fidelity evaluations; only two high-fidelity points are sampled, one of which is almost in the optimum location. Near the end of the sampling, most points are added around the optimum. FS on the other hand, uses more HF points spread around the parameter space. Not all these points are useful; note for example the set of points in the top left corner, where a second minimum was suspected in the initial stages of the sampling. And while the data points are clustered, none are placed directly around the optimum.

These differences are also reflected in the $\mathbf{x}^\star$ convergence (Fig. 6c). The CC of evaluating the startset is 7.35 for FS and only 1.24 for RS-MSE which, combined with the efficient initial LF exploration, means that RS-MSE has globally identified the optimum before FS finishes half its startset. The subsequent RS-MSE convergence is fast and without oscillations, as medium- and high-fidelity points are added around the optimum. The optimization has converged around $CC = 15$. The FS convergence is much more irregular, as it identifies two incorrect optima before finally settling on the correct one around $CC = 24$.

Table 1: DTMB 5415 SDDO problem, summary of the results.

Approach	CC	x_1	x_2	$\Delta_x\%$	$\Delta_f\%$	$\lvert E_p\rvert\%$	$\mathcal{J}_1$	$\mathcal{J}_2$	$\mathcal{J}_3$
FS	24.0	0.5506	0.1330	26.2	-4.5	1.73	16	18	72
RS-MSE	18.4	0.5043	0.1525	37.2	-4.9	0.87	3	44	103

Table 1 summarizes the performance of the FS and RS-MSE approaches. Although the CC is lower, the RS-MSE approach correctly identified the region of the minimum, using more low- and medium-fidelity data than the FS approach. The prediction error is twice lower, which confirms that the metamodel is accurate around the optimum. The $\Delta_x\%$ value is larger for RS-MSE

than for FS, meaning that the exploration for the identification of the minimum moved further. Finally, the RS-MSE approach achieves a lower resistance than the FS approach. Altogether, the RS-MSE optimization produces a similar optimum as the old FS result, in a more robust manner, for a total wall clock time that has reduced from 25 to about 11 days.

6 CONCLUSIONS

This paper focuses on assessing the efficiency of an adaptive multi-fidelity method for simulation-driven design optimization. Notably, the tests concern the reduced startset (RS) with one single point for all the fidelities except the lowest one, and the improved fidelity sampling, by subtracting the mean-squared error (MSE) between the training set and the least-squares regression, from the uncertainty on each fidelity level while selecting the fidelity to sample.

Numerical results show that the RS approach is effective in improving the identification of the minima and better distributing the high-fidelity samples in interesting regions of the domain. It encourages early exploration with low-fidelity samples, unconstrained by high-fidelity data which may wrongly indicate sub-optimal regions. This early exploration leads to a reliable identification of the minimum region. Later on, thanks to the limits imposed on the extrapolated high-fidelity uncertainty, sampling of high-fidelity data in the observed minimum region is encouraged, which efficiently increases the precision in the minimum region.

For the analytical test case, the RS-MSE approach achieves even better results than the RS approach, since its formulation is effective in forcing the fidelity selection towards the high-fidelity after a large number of low-fidelity evaluations have been performed. This is necessary for this case, since the low- and high-fidelity optima are in different locations. Finally, the DTMB 5415 SDDO problem shows that the RS-MSE method is highly effective in identifying the region of the minimum, performing high- and medium-fidelity evaluations almost exclusively in this region. Although few high-fidelity points are added, it is likely that the sampling with (accurate yet cost-effective) medium-fidelity points is encouraged by the RS-MSE.

In conclusion, the test results are promising, showing that the two developments tested specifically here, have a beneficial effect on the metamodel performance. Similar tests in our earlier papers have indicated the same for the other aspects of our surrogate modeling approach, such as the ACAS adaptive sampling and the LS-RBF noise-filtered metamodel. Thus, all these methods contribute to our eventual goal of achieving fully adaptive automatic multi-fidelity surrogate modelling.

ACKNOWLEDGMENTS

CNR-INM is partially supported by the Office of Naval Research through NICOP grant N62909-21-1-2042, administered by Dr. Elena McCarthy and by Dr. Woei-Min Lin of the Office of Naval Research Gobal and the Office of Naval Research, respectively. The work is conducted in collaboration with NATO STO AVT task group on "Goal-driven, multi-fidelity approaches for military vehicle system-level design" (AVT-331).

REFERENCES

[1] P. Anselma, C. B. Niutta, L. Mainini, and G. Belingardi. Multidisciplinary design optimization for hybrid electric vehicles: component sizing and multi-fidelity frontal crashworthiness.

Structural and Multidisciplinary Optimization, 62(4):2149–2166, 2020.

[2] M. Durand. *Light and flexible Fluid/Structure Interaction, application to sailing boats.* Thesis, Ecole Centrale de Nantes (ECN), Oct. 2012.

[3] S. Ficini, U. Iemma, R. Pellegrini, A. Serani, and M. Diez. Assessing the performance of an adaptive multi-fidelity gaussian process with noisy training data: A statistical analysis. In *AIAA Aviation Forum 2021*, page 3098, 2021.

[4] S. Lloyd. Least squares quantization in PCM. *IEEE transactions on information theory*, 28(2):129–137, 1982.

[5] R. Pellegrini, A. Serani, M. Diez, M. Visonneau, and J. Wackers. Towards automatic parameter selection for multifidelity metamodels. In *9th Conference on Computational Methods in Marine Engineering (Marine 2021)*, pages 2–4, online, 2021.

[6] P. Queutey and M. Visonneau. An interface capturing method for free-surface hydrodynamic flows. *Computers & Fluids*, 36(9):1481–1510, 2007.

[7] M. P. Rumpfkeil and P. S. Beran. Multi-fidelity, gradient-enhanced, and locally optimized sparse polynomial chaos and kriging surrogate models applied to test problems. In *AIAA Scitech Forum*, online, 2020.

[8] A. Serani, M. Diez, J. Wackers, M. Visonneau, and F. Stern. Stochastic shape optimization via design-space augmented dimensionality reduction and RANS computations. In *2019 AIAA/ASCE/AHS/ASC Structures, Structural Dynamics, and Materials Conference*, San Diego, USA, 2019.

[9] A. Serani, C. Leotardi, U. Iemma, E. F. Campana, G. Fasano, and M. Diez. Parameter selection in synchronous and asynchronous deterministic particle swarm optimization for ship hydrodynamics problems. *Applied Soft Computing*, 49:313 – 334, 2016.

[10] A. Serani, R. Pellegrini, J. Wackers, C.-E. Jeanson, P. Queutey, M. Visonneau, and M. Diez. Adaptive multi-fidelity sampling for CFD-based optimisation via radial basis function metamodels. *International Journal of Computational Fluid Dynamics*, 33(6-7):237–255, 2019.

[11] Y. Song, Q. S. Cheng, and S. Koziel. Multi-fidelity local surrogate model for computationally efficient microwave component design optimization. *Sensors*, 19(13):3023, 2019.

[12] S. Volpi, M. Diez, N. Gaul, H. Song, U. Iemma, K. K. Choi, E. F. Campana, and F. Stern. Development and validation of a dynamic metamodel based on stochastic radial basis functions and uncertainty quantification. *Structural and Multidisciplinary Optimization*, 51(2):347–368, 2015.

[13] J. Wackers, G. Deng, E. Guilmineau, A. Leroyer, P. Queutey, M. Visonneau, A. Palmieri, and A. Liverani. Can adaptive grid refinement produce grid-independent solutions for incompressible flows? *Journal of Computational Physics*, 344:364 – 380, 2017.

[14] J. Wackers, M. Visonneau, S. Ficini, R. Pellegrini, A. Serani, and M. Diez. Adaptive N-fidelity metamodels for noisy CFD data. In *AIAA Aviation Forum*, online, 2020.

[15] J. Wackers, M. Visonneau, A. Serani, R. Pellegrini, R. Broglia, and M. Diez. Multi-fidelity machine learning from adaptive- and multi-grid RANS simulations. In *33rd Symposium on Naval Hydrodynamics*, Osaka, Japan, 2020.